Materials Horizons RSCPublishing

Electronic Supplementary Information

Linker-Free Grafting of Fluorinated Polymeric Cross-linked Network Bilayers for Durable Reduction of Ice Adhesion

Hossein Sojoudi,[a,b] Gareth H. McKinley*[b] and Karen K. Gleason*[a]

[a]*Department of Chemical Engineering, Massachusetts Institute of Technology, 77 Massachusetts Avenue, Cambridge, MA 02139, United States*
E-mail: kkg@mit.edu

[b]*Department of Mechanical Engineering, Massachusetts Institute of Technology, 77 Massachusetts Avenue, Cambridge, MA 02139, United States*
E-mail: gareth@mit.edu

1. iCVD polymer coatings

In-situ grafting (process A) and iCVD polymerizations (process B) were carried out in a custom-built cylindrical reactor (diameter 24.6 cm and height 3.8 cm), subsequently an array of 14 parallel chromoalloy filaments (Goodfellow) suspended 2 cm from the stage.[36, 37] The reactor was covered with a quartz top (2.5 cm thick) that allows real-time thickness monitoring by reflecting a 633 nm He-Ne laser source (JDS Uniphase) off the substrate/polymer and recording the interference signal intensity as a function of time. The reactor was pumped down by a mechanical Fomblin pump (Leybold, Trivac) and the pressure was monitored with a MKS capacitive gauge. The liquid monomers (1H, 1H, 2H, 2H-perfluorodecyl acrylate, PFDA, 97% Aldrich) and (divinylbenzene, DVB, 80% Aldrich) and the initiator (*tert*-butyl peroxide, TBPO, 98% Aldrich) were used as received without further purification. TBPO was kept at room temperature (T_f= 25 ºC) and was delivered into the reactor through a mass flow controller (1479 MFC, MKS

Instruments) at a constant flow rate of 3 sccm in process A, and 3 sccm and 1 sccm in DVB and PFDA polymerization during process B, respectively. Methyl radicals were formed through heating the filaments at T_f = 310ºC during process A using a DC power supply (Sorensen), whereas initiator radicals (TBO) were created by breaking only the labile peroxide bond of the TBPO at filament temperature of T_f=250ºC during process B. PFDA and DVB were vaporized in glass jars that were heated to 80ºC and 60ºC, respectively and then introduced to the reactor through needle valves at constant flow rates of 0.1 and 1 sccm, respectively. The substrate temperature was kept at T_s = 20ºC in process A and 30ºC in process B (within ±1 ºC) using a recirculating chiller/heater (NESLAB RTE-7). All of the temperatures were measured by K-type thermocouples (Omega Engineering). The working pressure was maintained at 800 mTorr in process A and 800 mTorr and 100 mTorr in DVB and PFDA polymerization during process B, respectively, using a throttle valve (MKS Instruments). Prior to in-situ grafting, silicon wafers (Wafer World Inc.) and steel coupons (McMaster-Carr) substrates were first cleaned by sonication in acetone and isopropanol each for 5 minutes, followed by rinsing in DI water (>16 MOhm-cm). The surfaces were then treated with oxygen plasma for 10 minutes for further cleaning and for creating surface hydroxyl groups prior to transfer into iCVD reactor.

2. FTIR spectra of iCVD coatings

FTIR were performed on a Nicolet Nexus 870 ESP spectrometer in normal transmission mode equipped with a MCT (mercury cadmium tellurium detector and KBr beamsplitter). Spectra were acquired over the range of 500 to 4000 cm^{-1} with a 4 cm^{-1} resolution for 256 scans.

Fig. S2 shows FTIR spectra of pDVB, pPFDA, and linker-free grafted bilayer pDVB/pPFDA polymer with a top layer pPFDA thickness of 10 nm (LFG-BL (10 nm)). A sharp band located at 1741 cm^{-1}, corresponding to carbonyl group, two sharp bands at 1207 and 1246

cm^{-1}, caused by the asymetric and symetric stretching of $–CF_2$-, and a band at 1153 cm^{-1}, belonging to the –CF2-CF3- end group, are all characteristics of the pPFDA. The spectra for the pDVB shows a band between 3000 and 3100 cm^{-1}, corresponding to the aromatic –CH- band, another band between 2810 and 2890 cm^{-1}, the –CH2- streatching band, and additional bands in the range of 700-1000 cm^{-1}, all related to the substituted phenyl group. It has to be noted that the corresponding bands in the pDVB spectra are less intense when compared to the pPFDA and can only be seen clearly in the expanded image. The increase in the top layer pPFDA thickness to 40 nm results in significantly less intensity for the FTIR peaks corresponding to the underlying pDVB. FTIR spectra of the LFG-BL (10 nm) indicate the presence of all characteristics bands associated with the pDVB and the pPFDA. FTIR spectras also showed identical results for the LFG-BL, linker grafted bilayer pDVB/pPFDA (LG-BL), and ungrafted bilayer pDVB/pPFDA (UG-BL) polymer with pPFDA thickness of 10 nm indicating full retention of the all functional groups.

3. XPS spectra of iCVD coatings

X-ray data was acquired using a spectrophotometer (PHI 5000*VersaProbe* II) with an Al Kα X-ray source. The survey scan spectra were collected at binding energies (B.E.) of 200-800 eV with a step size of 0.8 eV, a pass energy of 187.8 eV, a take-off angle of 45°, and a spot size of 200 μm. Figure S3 (a) shows survey scan spectra randomly collected from BL (10 nm) on Si. The scan showed the most prominent peaks to be C1s, O1s, and F1s. The appearance of an F1s peak centered at 688.4 eV confirms the presence of fluorine groups on the bilayer film. High resolution XPS spectra of F1s and C1s binding energy were also acquired over binding energy of 680-693 eV and 282-295 eV, respectively (Figure S3 (b) and (c)). For high resolution, the instrument was utilized in a high power mode with a raster scan of 100 μm spot over a line of 1.4 mm long. The

pass energy and step size for high resolution spectra were 23.5 eV and 0.1 eV, respectively. Each measurement was examined in several spots to ensure reproducibility. Multipack software was utilized for analysis of the collected spectra, where 70% Gaussian-30% Lorentzian curve fitting was performed. The C1s XPS spectrum can be described using the five bonding environments expected due to vinyl polymerization of the PFDA monomer. Table S1 shows the position of each peak and its comparison to the theoretical values.

4. Details of mechanical measurements

A Nanovea mechanical tester (M1 P-Nano/AFM) was used for the nanoindentation and nanoscratch experiments. The indenter-microscope calibration was performed using a copper sample with a maximum load of 20 mN and indenter approach speed of 30 μm/min. Depth and compliance calibration was performed on a fused silica sample with a Young's modulus of 72 GPa and Poisson's ratio of 0.17. A conical diamond indenter tip (Young's modulus = 1140 GPa and Poisson's ratio = 0.07) with a radius of R=10 μm was used during all indentations. All of the polymer films used in the nanoindentation experiments were more than 1 μm thick. This was achieved by increasing the thickness of pDVB, while keeping the pPFDA thickness in the same range (10 or 40 nm thick) depending on the desired wettability properties. A maximum indentation depth of 25-150 nm was used to eliminate the possibility of substrate effects which complicate the subsequent analysis. In addition, exploratory tests were performed to ensure that the normal load did not experience a sudden change by a slight increase in the maximum penetration depth indicating that any underlying substrate effect was very minimal. A 4 × 4 grid was used during the indentation of the polymers, with 10 μm separation in both directions between indentations.

The ASTM E2546 (ISO 14577) procedure was used by the software to obtain elastic modulus and hardness of the polymers for 16 indentations per sample. Maximum load, load rate, and the creep time were changed to evaluate the time response to loading of the polymers. Finally, a maximum load of 0.38 mN with 0.8 mN/min rate and creep time of 5-60 seconds (depending on the polymer film being tested), were applied throughout the indentation measurements. This ensured appropriate deformation of the polymer networks during loading/unloading cycles and enabled a linear fit to the load-penetration curves during unloading. The Poisson's ratio for all of the polymers was assumed to be the same and equal to 0.5.[28] A contact load of 0.05 mN was used during the nanoindentation measurements and the recording of the data were stopped once the normal load reached the contact load (Fig. 2a).

5. Calculating the area function ($A(h_c)$) from the indentation curve

The contact Area $A(h_c)$ is calculated by evaluating the indenter area function. This function will depend on the diamond geometry and at low loads by an area correction. A power-law fit through the upper 1/3 to1/2 of the unloading data intersects the depth axis at h_t (Fig. S3). The stiffness, *S*, is given by the slope of this line. The contact depth, h_c, is then calculated as:

$$h_c = h_{max} - \frac{3P_{max}}{4S} \qquad \text{(S1)}$$

The contact Area, $A(h_c)$, is calculated by evaluating the indenter area function. This function will depend on the diamond geometry and at low loads by an area correction. For a spherical indenter, the area function is $A(h_c) = 2\pi R h_c$ where R is the radius of the indenter.

The minimum creep time required to ensure proper deformation of the polymer during loading/unloading was 60 seconds for pPFDA, 10 seconds for pDVB, and 5 seconds for LG-BL and LFG-BL. To ensure accuracy, the measurement on the pPFDA surface was repeated at

different maximum load (P_{max}= 0.3 mN) with the same load rate (0.8 mN/min). A 50 seconds creep time was found to be enough to obtain the desired shape for the load-penetration curve during unloading (Fig. S5). This measurement resulted in elastic modulus and hardness values of 7.0 GPa and 125.1 MPa for the pPFDA, respectively, which are within the same range of the values obtained in the previous set of the measurements with P_{max} of 0.4 mN (E_{pPFDA}=8.2±2.1 GPa and H_{pPFDA}=131.0±5.7 MPa, Table S1).

6. Nanoscratch measurements

Nanoscratch measurements were performed on each polymer film with a minimum thickness of 1 μm at multiple spots with at least 50 μm separations (N≥4) to ensure repeatability. A maximum load of 0.5 mN with a load rate of 1 mN/min was applied using a 10 μm radius tip to create 2 mm long scratches. A maximum load of 0.5 mN with a load rate of 1 mN/min was applied using a 10 μm radius tip to create 2 mm long scratches. For the grafted polymer networks, a maximum load of 5 mN was applied while the scratch length was kept at 2 mm resulting in much higher load rate (1.238 mN/min) for these nanoscratch tests to simulate severe conditions.

7. Surface morphology measurements

Surface film morphology was investigated by atomic force microscopy (AFM–Digital Instruments, D3100-1). Images were acquired in tapping mode in air using conical gold-coated silicon tips. Deposited trench wafers were sputter-coated with 5 nm of gold (Denton Desk V), and images were obtained by SEM (JEOL 6010LA) with an acceleration voltage of 5 kV. For SEM-EDS, the acceleration voltage was adjusted to allow mapping without charge accumulation and drift of the images during the mapping. The black and white SEM image is intentionally out of clear focus to optimize the EDS analysis. The black and white images are computer-colored with assigned color schemes for specific elements. These images reveal that C and F are uniformly

distributed in the bilayer film. A '+' crossmark was intentionally created on the sample prior to SEM-EDS to ensure EDS mapping with minimal drift in images, which can happen due to possible charge accumulation. A Zeta-20 non-contacting optical profilometer was used to investigate the surface morphology of the samples. The Zeta system scans a sample over a user-specified vertical (or Z) range on 136 μm × 102 μm surface areas. At each Z position, it records the XY location and the precise Z height of the pixels using the Zeta Optics Module. This information is used to create a true color 3D image and a 2D composite image. The Zeta 3D software was used to ascertain dimensional and roughness information. *Rq* is the root mean squared (RMS) of the roughness values obtained from the AFM and profilometer images. All RMS values averaged over an interrogation region. The actual surface area was obtained through surface integration of the AFM and optical profilometer measurements. The Wenzel roughness, *r*, was calculated by dividing the actual measured surface area over the projected geometric surface area.

8. Water contact angle measurements

Water contact angles (WCA) were measured using a goniometer equipped with an automated dispenser (Model 500, ramé-hart). Advancing and receding WCAs were measured with the sessile drop method by depositing a water droplet of 2-3 μL on the surface, then increasing the volume by 0.15 μL increments until advancement in the liquid meniscus was observed and then decreasing by the same rate until receding motion was seen. Advancing WCAs were considered as the maximum angles observed during the droplet growth, while receding WCAs were measured in correspondence of the drop profile just before the interface receded. WCA hysteresis was also calculated as the difference between the cosines of the measured receding and

advancing WCA. Each WCA and WCA hysteresis value was averaged from measurements of ten droplets distributed across the sample.

9. Ice adhesion measurements

The strength of ice adhesion was measured using a custom-built ice adhesion set up whose details are described elsewhere.[4, 12] The samples were cut into 1.5 cm × 1.5 cm pieces and clamped to a base plate. Then, plastic cuvettes with a 1 cm × 1 cm cross section ~90% filled with water were inverted on them and clamped. Care was taken to remove any possible water residue on the substrate around the cuvettes. The entire plate was cooled at a rate of 2°C per second from room temperature to −15°C on a Peltier plate (TECA Corporation, model LHP-800CP) in a low-humidity nitrogen atmosphere and was maintained at this temperature for at least 2h to ensure complete freezing of water within the cuvettes. The probe of a force transducer (Imada, model ZP-44) was used to apply a shear force to the cuvettes, and the maximum force required to fracture the ice−substrate interface was recorded. The probe was located about 1.3 mm above the substrate surface to minimize torque on the ice sample. This distance was maintained the same for all samples with the same substrate type (steel or silicon). The force measurement tests were performed on twenty samples of each type to minimize statistical variations. This variation might be partially due to differences in ice nucleation and growth dynamics between samples with similar coating.[55] The maximum measured forces at the ice-substrate break point were converted to a measure of the shear strength of ice adhesion by dividing over the known cross-section area of the ice-substrate interface (1 cm^2).

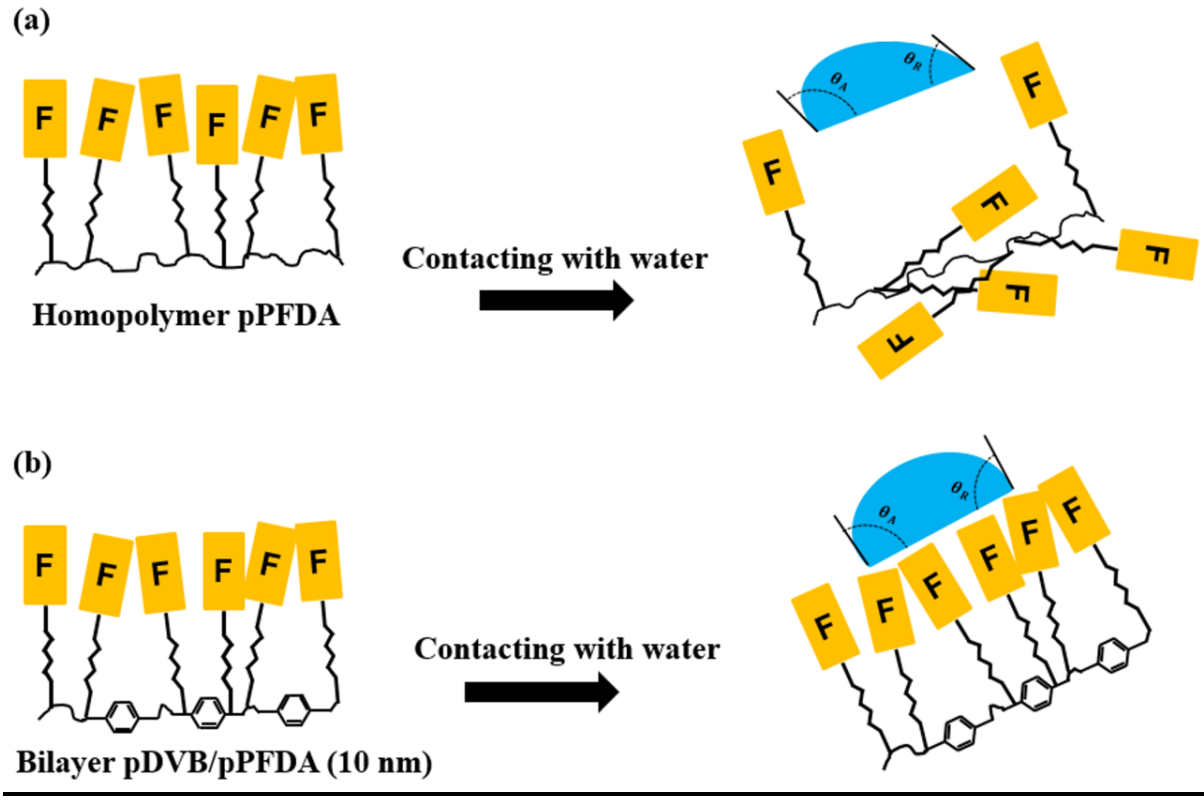

Fig. S1. Schematic of (a) homopolymer pPFDA and (b) bilayer pDVB/pPFDA with only 10 nm thick top layer pPFDA. The presence of highly cross-linked pDVB polymer layer underneath a very thin pPFDA fluoropolymer in (b) acts as a steric barrier resisting local surface reorganization, forcing the fluorinated groups to remain on the surface even under wet conditions.

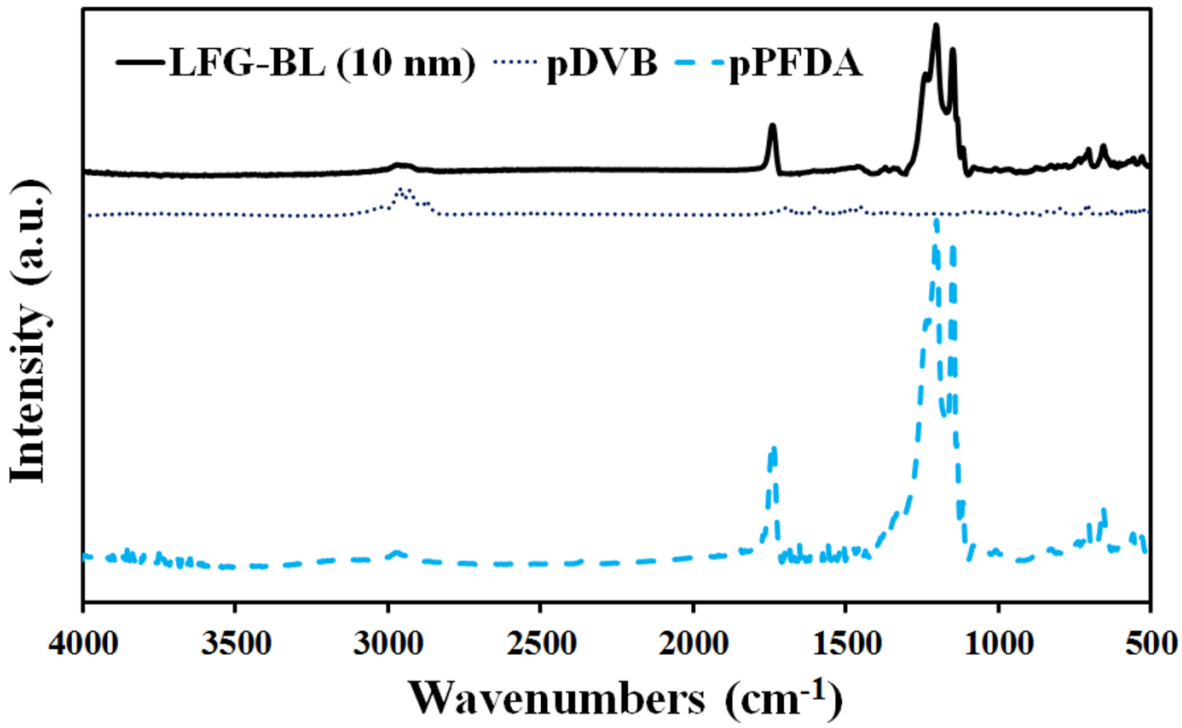

Fig. S2. Polymer composition determined by Fourier transform IR (FTIR) spectra of the pPFDA, pDVB, and linker-free grafted bilayer pDVB/pPFDA with 10 nm top layer pPFDA thickness (BL (10 nm)). Presence of the bands corresponding to carbonyl (at 1741 cm^{-1}) and fluorine (at 1153, 1207, and 1246 cm^{-1}) in the pPFDA spectra and band corresponding to phenyl group (in the range of 700-1000 cm^{-1}) in the pDVB spectra is indicative of succesful deposition of these polymers. All of these bands observed in the FTIR spectra of BL (10 nm) indicating prsence of the thin pPFDA on top of the pDVB in the bilayer polymer.

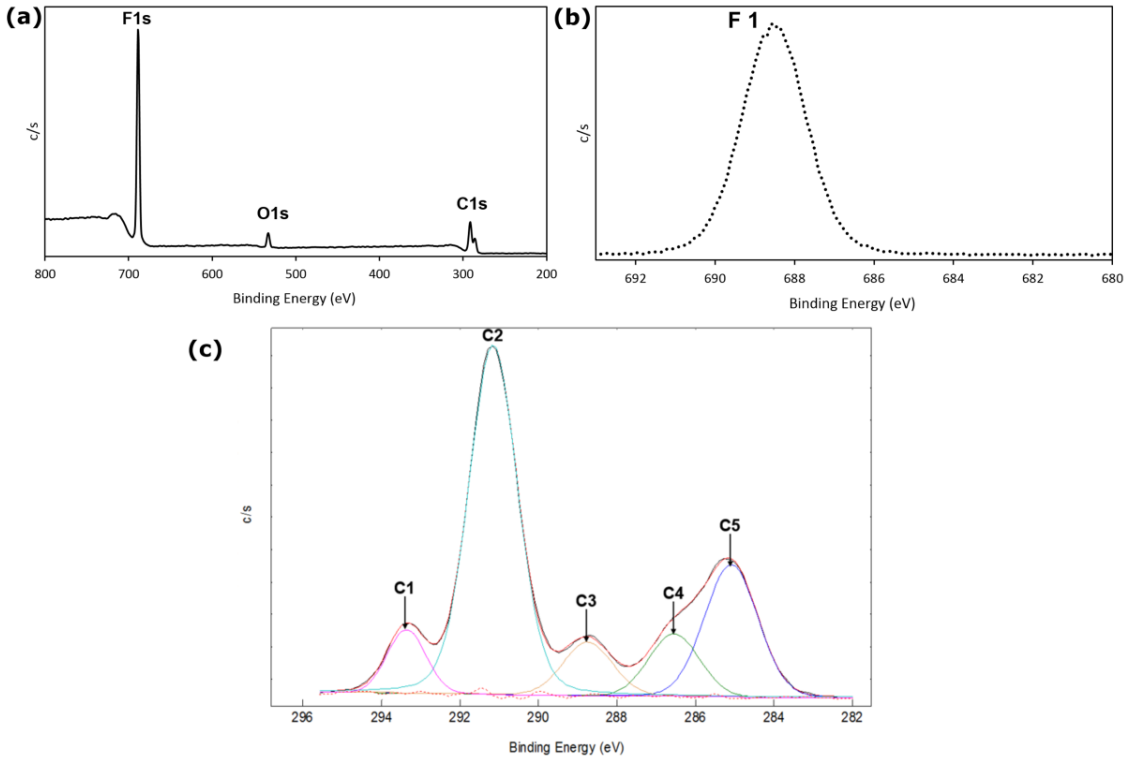

Fig. S3. (a) XPS survey spectra for detection of the atomic concentration of fluorine, oxygen, and carbon. (b) F1s high resolution XPS centered at 688.4 eV indicates the presence of fluorine groups. (c) High resolution C1s spectra with five resolved peaks (C1: -C*F_3, C2: -C*F_2, C3:-C*=O, C4: -O-C*H_2-CH_2-, C5: -C-C*H_2-C-).

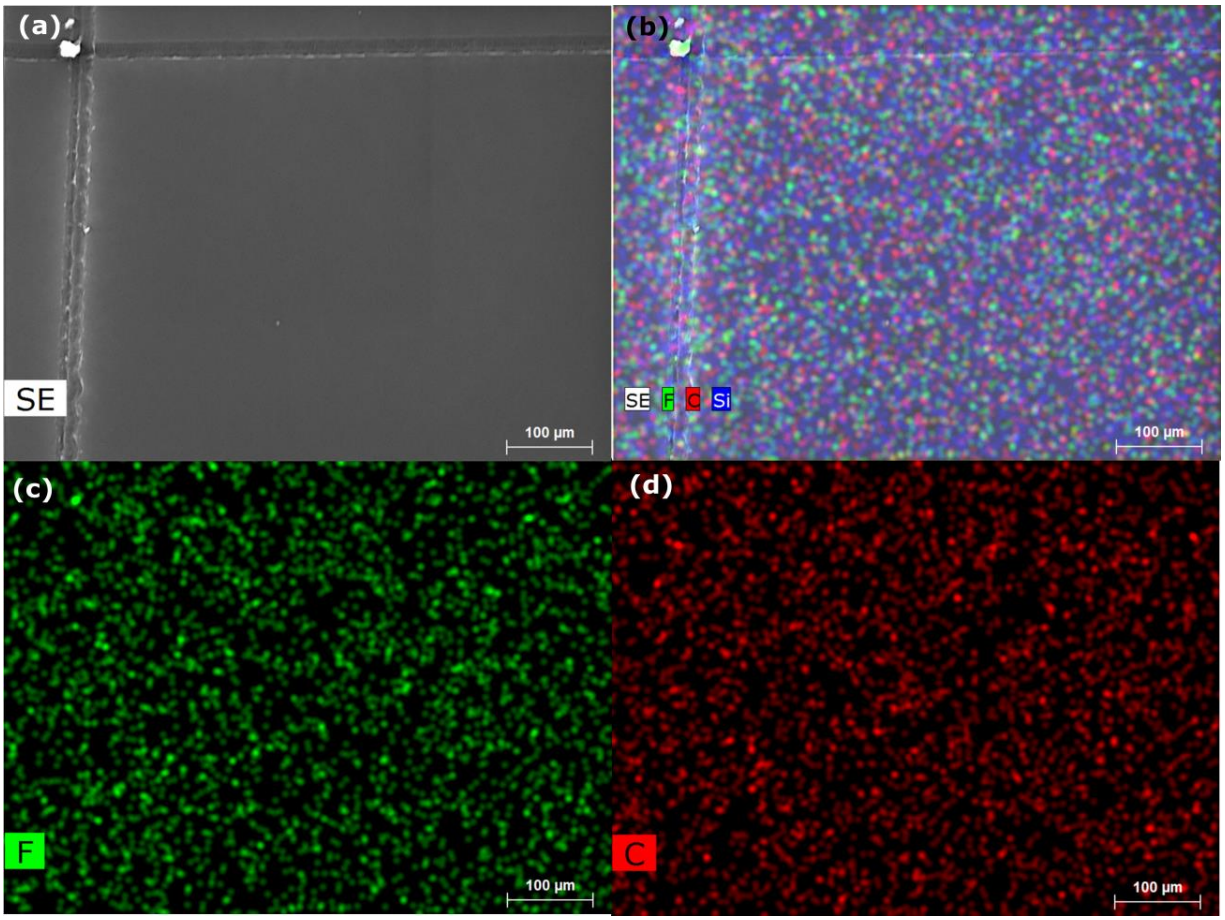

Fig. S4. (a) SEM-EDS micrograph and maps of distribution of elements on the linker-free grafted bilayer pDVB/pPFDA with pPFDA thickness of ~ 10 nm deposited on the silicon substrate (BL (10 nm) on Si). The '+' mark is used as a fiducial reference to ensure that there is minimal drift in the images. The secondary electron (SE) image with Si, C, and F mapping in (b). The images in (c) and (d) reveal that carbon and fluorine species are uniformly distributed in the bilayer film.

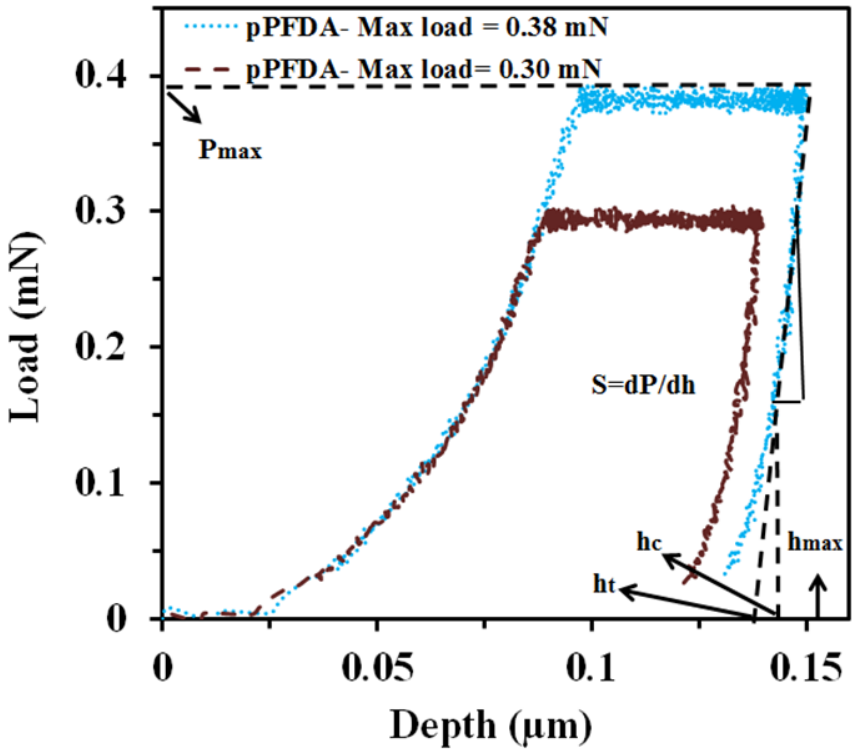

Fig. S5. Load/depth curves obtained from the nanoindentation measurements on the pPFDA film using 0.38 mN and 0.3 mN maximum load. The stiffness, *S*, is given by the slope of the unloading curve.

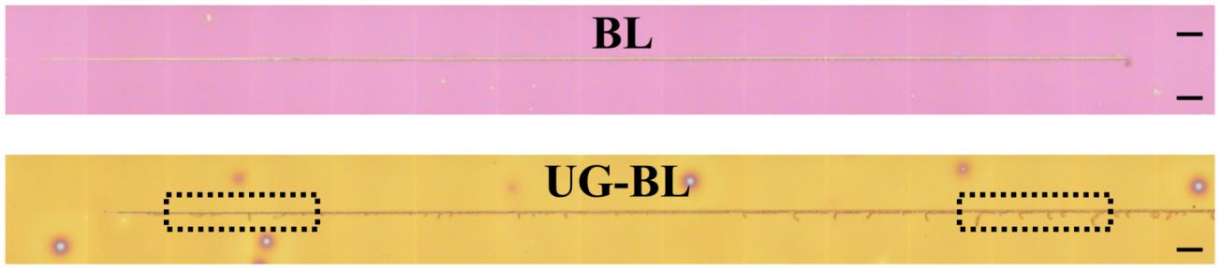

Fig. S6. Optical microscopy images obtained from the Nanovea mechanical tester after creation of a 2 mm long scratch on linker-free grafted bilayer pDVB/pPFDA (BL) (top) and ungrafted bilayer pDVB/pPFDA (UG-BL) (bottom). The UG-BL shows that the polymer delaminated frequently during the nanoscratch test while grafted polymers did not experience any sign of failure. The scale bar is 50 μm.

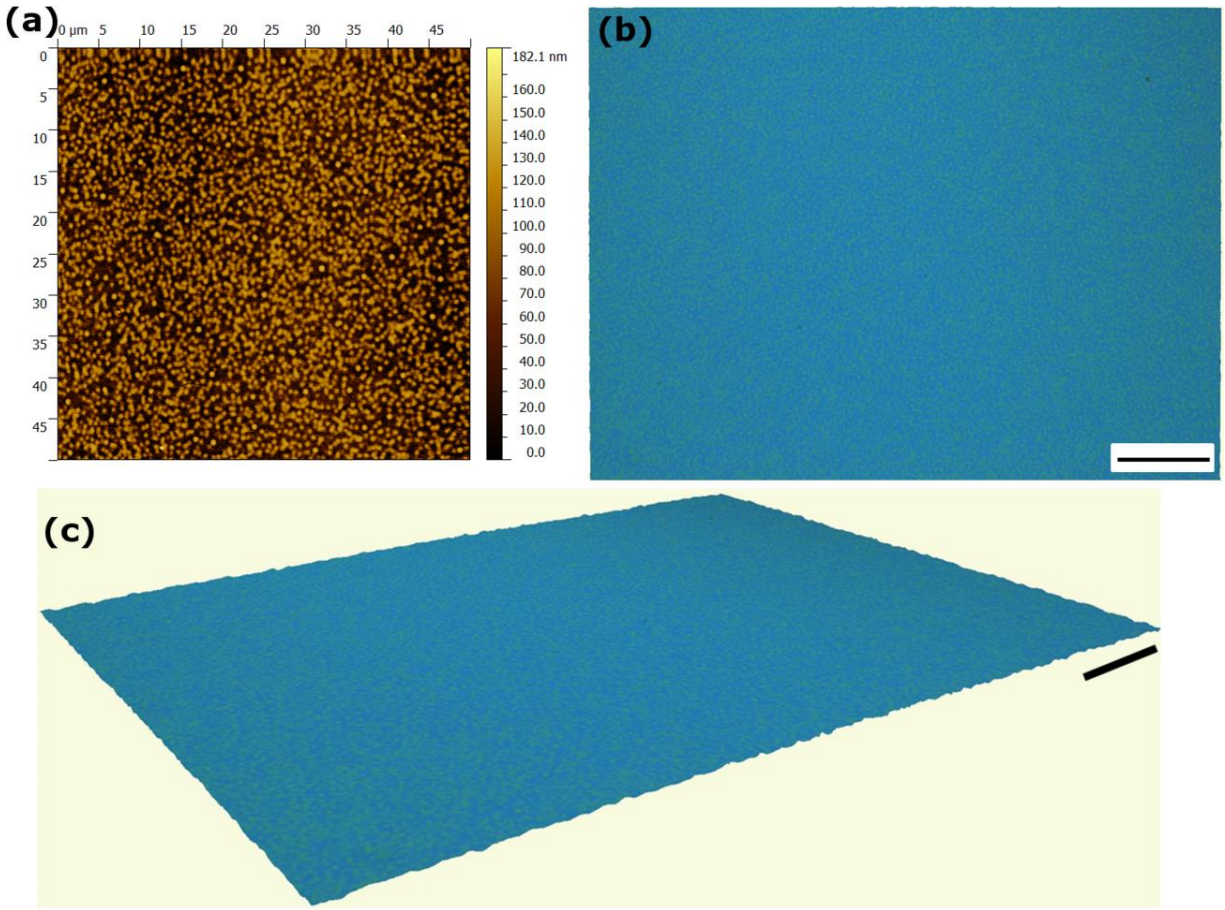

Fig. S7. (a) is AFM image, (b) and (c) are the top view and three dimensional optical profilometer images of the linker-free grafted bilayer pDVB/pPFDA with pPFDA thickness of ~ 10 nm deposited on the silicon substrate (BL (10 nm) on Si), respectively. AFM, and optical profilometer images show the presence of rough features in the BL (10 nm) on Si film with RMS roughness of R_q=28.3±3.8 nm. The scale bars in (b) and (c) are 20 µm.

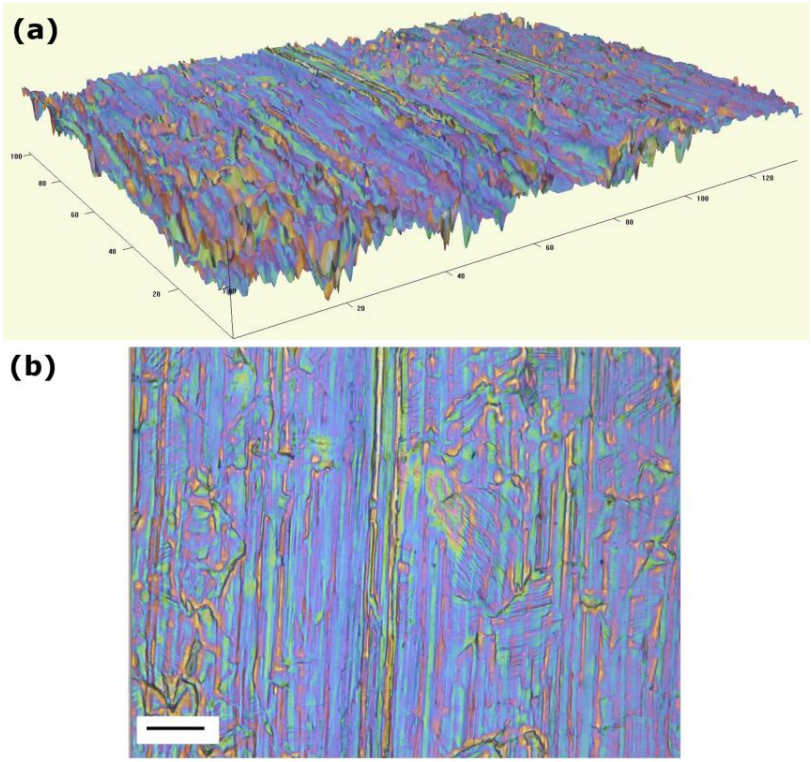

Fig. S8. Three dimensional (a) and top view (b) optical profilometer images of the linker-free grafted bilayer pDVB/pPFDA with pPFDA thickness of ~ 10 nm deposited on the steel substrate (BL (10 nm) on steel). Features observed in the images are mainly due to the underlying rough steel substrate on which the polymer was deposited (RMS value of R_q=120.3±22.0 nm). The images were taken over 136 μm × 102 μm imaging area. The vertical (Z) scale is exaggerated in (a); the scale bars represent 15 μm in (b).

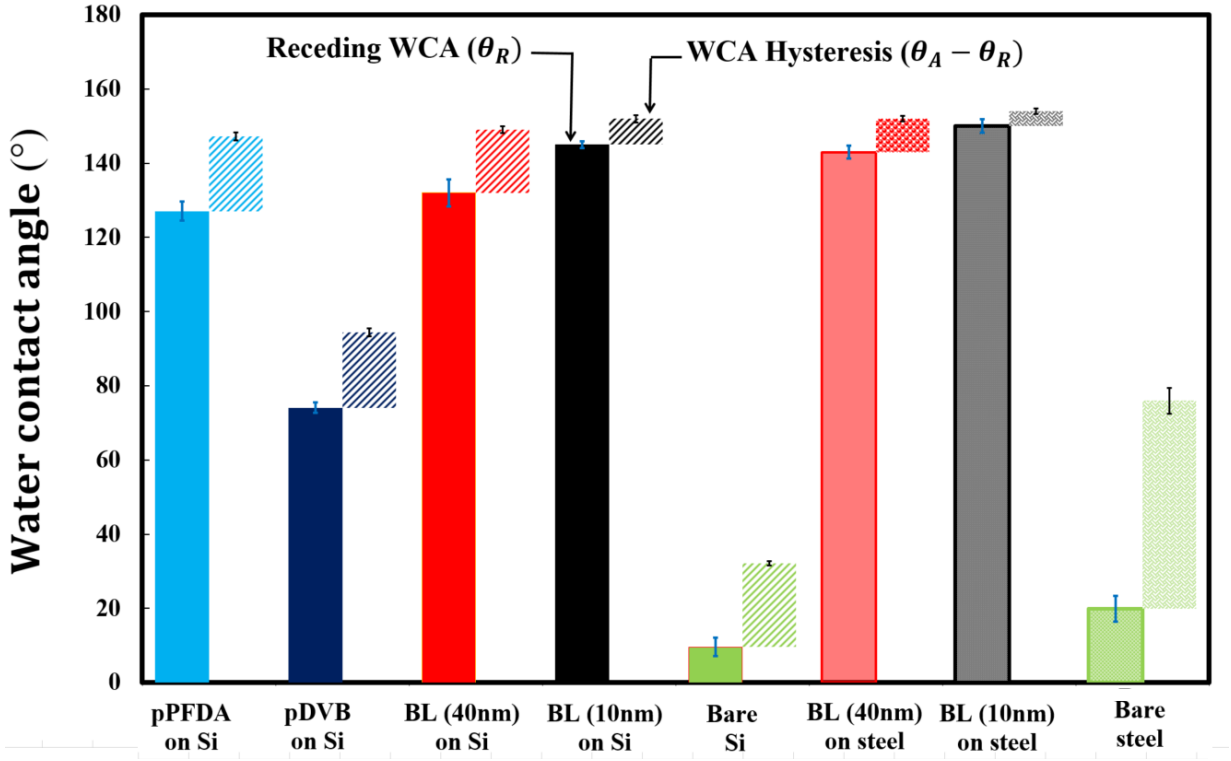

Fig. S9. Water contact angle (WCA) measurements of the polymers deposited onto silicon and steel substrates. Filled bars are the receding WCAs (θ_R) while the patterned bars show the WCAs hysteresis ($\theta_A - \theta_R$). Bilayer polymers deposited on steel substrates show lower contact angle hysteresis when compared to those deposited on silicon; this is due to the rough steel substrate which promotes Cassie-Baxter wetting state. A thinner pPFDA (~ 10 nm) in a bilayer film deposited on a given substrate (BL (10 nm) on steel or silicon) resulted in lower WCA hysteresis when compared to a thicker pPFDA (~ 40 nm) top layer; this is due to the presence of very dense pDVB network underneath, which prevents inwards reorientation of the fluorine groups in the pPFDA coating once exposed to water during WCA measurements (see Fig. S1).

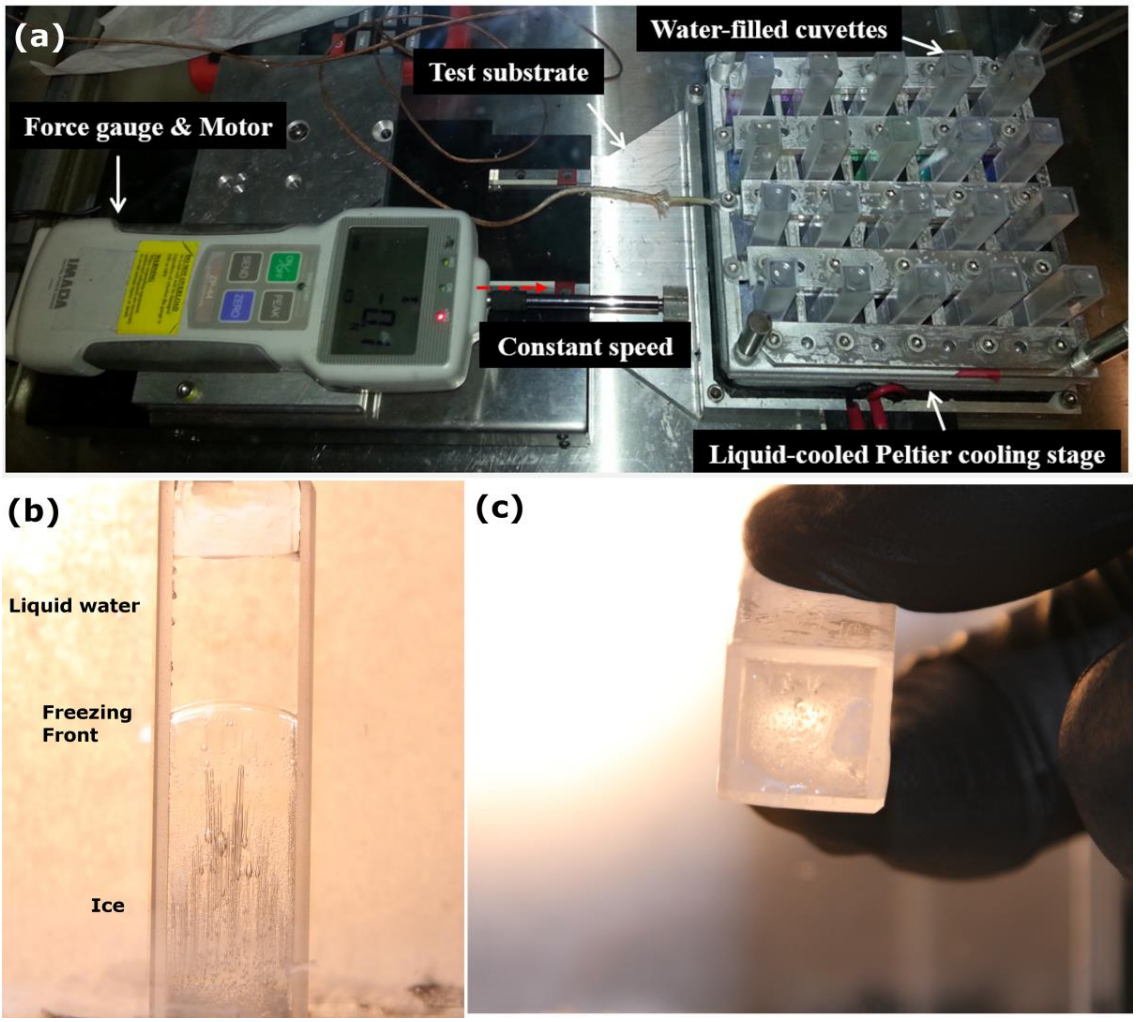

Fig. S10. (a) Photograph of the ice adhesion test apparatus showing 90% water-filled cuvettes that are inverted on test substrates and cooled at -15ºC using a Peltier cooling stage for 2h to promote ice formation. (b) Image of ice being formed inside a cuvette and the solidification front. (c) Image of a cuvette after de-adhering from the substrate showing the state of the ice formed on the substrates and the smooth fracture interface.

Table S1. Atomic percentage of carbon, oxygen, and fluorine obtained from XPS survey spectra and binding energy of carbon environments from C1s high resolution XPS. The values obtained from the XPS measurements are in good agreement with the theoretical data.

	Carbon (C1s) %	Oxygen (O1s) %	Fluorine (F1s) %	$-C^*F_3$ B.E. (eV)	$-C^*F_2$ B.E. (eV)	$-C^*=O$ B.E. (eV)	$-O-C^*H_2-CH_2-$ B.E. (eV)	$-C-C^*H_2-C-$ B.E. (eV)
Theoretical	40.6	6.2	53.1	293.3	291.2	289.2	286.7	285.0
Experimental	39.6	5.1	55.3	293.3	291.2	288.7	286.2	284.9

Table S2. Wettability and icephobic properties of the linker-free grafted bilayer pDVB/PPFDA with ~ 10 nm pPFDA (BL (10 nm) on Si and steel) were characterized on as-deposited coatings and after ice adhesion test (ice formation and detachment). These data indicate that the icephobic coatings developed in the present work are durable to de-adhesion events.

	As-deposited		After Ice Adhesion Test	
	BL (10 nm) on Si	**BL (10 nm) on steel**	**BL (10 nm) on Si**	**BL (10 nm) on steel**
θ_A (°)	152.0±1.0	154.2±2.2	146.8±5.3	148.7±6.7
θ_R (°)	145±1.8	150.3±1.6	139.2±8.5	148.1±4.4
Ice Adhesion Strength (kPa)	185.3±83.7	158.5±76.0	208.2±105.0	171.5±92.7

Table S3. Mechanical properties (hardness and elastic modulus) obtained from nanoindentation measurements. Root mean squared roughness, *Rq*, obtained from optical profilometer measurements. Receding water contact angle (WCA) and WCA hysteresis measured using a goniometer equipped with an automated dispenser, and ice adhesion strength data measured on silicon and steel coated substrates using a custom-built ice adhesion set up. The data provided in the table suggest that linker-free grafted bilayer pDVB/pPFDA (BL (10 or 40 nm)) has better mechanical properties. The ice adhesion strength was reduced six-fold on the silicon and steel substrates coated with BL (10 nm) when compared to bare silicon and steel.

Sample	Hardness (MPa)	Elastic Modulus (GPa)	Root mean squared R_q(nm)	Receding WCA θ_R (°)	WCA Hysteresis (°)	Ice adhesion strength (kPa)
pPFDA	131.0±5.7	8.2±2.1	15.5±3.4	127.1±5.2	20.1±1.1	272.8±120.2
pDVB	390.1±4.0	15.7±1.5	16.1±2.2	74.1±2.9	20.3±1.0	845.0±85.7
BL (40 nm) on Si	479.0±7.0	19.1±1.2	34.2±5.2	132.0±7.8	17.1±0.9	240.0±109.3
BL (10 nm) on Si	-	-	28.3±3.8	145.0±1.8	7.0±1.0	185.3±83.7
BL (40 nm) on steel	-	-	132.5±17.4	143.2±1.7	9.1±0.8	192.3±68.6
BL (10 nm) on steel	-	-	120.3±22.0	150.3±1.6	3.9±0.7	158.5±76.0